Technical Reference on Hydrogen Compatibility of Materials

High-Alloy Ferritic Steels:
Ferritic Stainless Steels (code 1500)

Prepared by:
C. San Marchi, Sandia National Laboratories
and
J.A. Zelinski, Defense Nuclear Facilities Safety Board, Washington DC

Editors
C. San Marchi
B.P. Somerday
Sandia National Laboratories

This report may be updated and revised periodically in response to the needs of the technical community; up-to-date versions can be requested from the editors at the address given below or downloaded at http://www.ca.sandia.gov/matlsTechRef/ . The success of this reference depends upon feedback from the technical community; please forward your comments, suggestions, criticisms and relevant public-domain data to:

     Sandia National Laboratories
     Matls Tech Ref
     C. San Marchi (MS-9402)
     7011 East Ave
     Livermore CA 94550.

1. General

There are numerous classes of stainless steels, including ferritic, martensitic, austenitic, duplex, and precipitation-hardened. The ferritic stainless steels are distinguished by the primary alloying element, chromium, which provides a stable ferritic structure at all temperatures. Due to low carbon content, the ferritic stainless steels have limited strength but can have good ductility and work harden very little. The toughness of these alloys tends to be quite low and their ductile to brittle transition is at or above room temperature. The special ferritic alloys were developed for improved toughness and may contain molybdenum, providing them with corrosion resistance superior to austenitic stainless steels in most environments [1].

Ferritic stainless steel has high diffusivity and low solubility for hydrogen compared to austenitic stainless steels. Although the properties of ferritic alloys measured in hydrogen gas (particularly at high-pressure) are scarce in the literature, the general trends emerging from the literature are that the ferritic stainless steels are at least as susceptible to hydrogen-assisted fracture as the unstable austenitic stainless steels (e.g., type 301 and 304 stainless steels). NASA reports classify type 430F stainless steel as severely embrittled by high-pressure hydrogen gas [2, 3].

1.1 Composition

The ferritic stainless steels have anywhere from 10-30 wt% Cr, however, chromium typically ranges from 12-18 wt%. Special ferritic alloys are generally those that contain higher amounts of Cr with some containing as much as 24-30 wt%. Molybdenum is sometimes added to the ferritic stainless steels in the range 1-4 wt% and Ni, if present, is generally < 2 wt%. Carbon and nitrogen contents are generally low, as in the 300-series austenitic stainless steels. The compositional ranges of a number of ferritic stainless steels are given in Table 1.1.1. Table 1.1.2 lists the compositions of alloys used to study hydrogen effects.

1.2 Other Designations

The most common grades of ferritic stainless steels are known by their AISI designation, such as type 430 and 434 ferritic stainless steels. Type 400 series alloys also include a number of martensitic stainless steels, which are generally distinguished by their high strength and low resistance to hydrogen-assisted fracture in hydrogen gas [2, 3].

Some ferritic alloy designations can be easily confused with those of austenitic stainless steels. The so-called 18-2FM and 18Cr-2Mo, for example, are special ferritic stainless steels that are distinct from 18-2-Mn, which is an austenitic stainless steel containing 11-14 wt% Mn and up to 2.5 wt% Ni.

2. Permeability, Diffusivity and Solubility

Permeation and diffusion in 29Cr-4Mo-2Ni (29-4-2) have been studied by gas phase permeation experiments [4, 5] and by electrochemical diffusion studies [6, 7]. Hydrogen permeation in annealed 29-4-2 ferritic stainless steel was found to be one to two orders of magnitude greater than in austenitic stainless steels, with greater differences at low temperatures (Figure 2.1) [4, 5]. Hydrogen diffusivity of this steel was found to be 2 to 5 orders of magnitude greater than in austenitic stainless steels (Figure 2.2). Hydrogen solubility in the ferritic stainless steels is significantly less than for austenitic stainless steels (Figure 2.3).

A discontinuity in diffusivity is apparent at about 443 K, where diffusivity values at temperatures less than 443 K are lower than values extrapolated from diffusivity measurements at higher temperatures. Similar observations have been made for iron and ferritic steels, and this has been attributed to trapping of hydrogen at microstructural defects during transport of hydrogen in the lower temperature regime [8, 9]. In addition, it has been shown that the apparent diffusivity is a function of concentration of hydrogen in the lattice and the concentration of hydrogen in trapping sites [8]. At high temperature, hydrogen is not trapped due to the available thermal energy preventing the binding of hydrogen to trapping sites. Thus, the diffusivity correlation for temperatures greater than 443 K can be interpreted as the lattice diffusivity in the absence of hydrogen trapping. The apparent solubility of hydrogen (determined from the quotient of the permeability and the diffusivity) shows the effect of the diffusion discontinuity in the annealed material as well: at temperature lower than 443 K, the hydrogen solubility is higher than extrapolation from higher temperature solubility would predict. This implies that in the lower temperature regime the hydrogen in the material is a sum of hydrogen dissolved in the lattice and trapped hydrogen, while at higher temperatures where trapping is less effective, the amount of hydrogen in the material is primarily due to dissolution in the lattice.

Cold-working the 29-4-2 reduced hydrogen diffusivity by an order of magnitude or more [5]; a much larger change than observed for cold-worked austenitic stainless steels [4, 10, 11]. Deformation in ferritic steels increases the density of hydrogen trapping sites, therefore, cold-working would be expected to have a larger impact on the apparent hydrogen diffusivity compared to annealed materials (Figure 2.2). In addition, the effect of hydrogen trapping on diffusivity is extended to higher temperatures, presumably because hydrogen is bound to traps more strongly and more thermal energy is required to overcome the trapping. Permeation was also reduced by cold-working, by almost a factor of 10 (Figure 2.1). Cold-working increases the hydrogen solubility at low temperature (less than about 573 K), but it is similar to the annealed material at higher temperature (Figure 2.3). The parameters for predicting permeability, diffusivity and solubility are given in Table 2.1.

Elastic stress was found to change hydrogen diffusivity by less than 50% in the temperature range of 303 K to 353 K [6]. It appears that the magnitude of diffusivity is nominally unaffected by applied stress (a factor of 2 can be considered small for diffusion experiments), but the activation energy for diffusion increased. The partial molar volume of hydrogen in 29-4-2 was determined to be 2.3×10^{-6} m^3 mol^{-1} (mole of H atoms) from these electrochemical measurements [6].

3. Mechanical Properties: Effects of Gaseous Hydrogen

3.1 Tensile properties

3.1.1 Smooth tensile properties
A significant reduction in tensile ductility was reported for type 430F ferritic stainless steel (heat W69) [2, 3]. Smooth bar tensile tests were performed in 69 MPa helium and hydrogen gases respectively as summarized in Table 3.1.1.1.

3.1.2. Notched tensile properties

Notched round tensile specimens of type 430F ferritic stainless steel (heat W69) tested in high-pressure gas show ~30% loss of strength in hydrogen compared to helium gas, Table 3.1.2.1. This testing was performed as part of a large test program in which this ferritic stainless steel was classified as severely embrittled [2, 3].

Perng and Altstetter tested 29Cr-4Mo-2Ni (29-4-2, heat P87) ferritic stainless steel notched sheet specimens (where plane stress conditions prevailed) in air and 0.11 MPa hydrogen gas from 298 to 573 K [12]. These sheet specimens exhibited 17 percent reduction of notch tensile strength and a 50 percent loss of ductility. The effects were most severe at room temperature and gradually disappeared as the temperature increased above 373 K. The fracture mode changed from microvoid coalescence in air to fracture surfaces dominated by quasicleavage in hydrogen gas. For temperature above ambient, the amount of ductile features increases with temperature and at 423 K the fracture surfaces are similar to tests performed in air [12].

3.2 Fracture mechanics

3.2.1 Fracture toughness

No known published data in hydrogen gas.

3.2.2 Threshold stress intensity

Perng and Altstetter determined crack growth rates and threshold stress intensity factor values in sustained load testing for 29-4-2 ferritic stainless steel (heat P87) notched sheet specimens where plane stress conditions prevailed [12]. The specimens were tested in air and 0.11 MPa hydrogen gas from 298 to 373 K [12]. The testing showed the threshold stress intensity factor increased with temperature, but the crack growth rate was generally higher at elevated temperature. This is rationalized in terms of hydrogen transport and accumulation ahead of the crack tip [12].

Huang and Altstetter also determined crack growth rates and threshold stress intensity factor values in the same 29-4-2 ferritic stainless steel (heat P87) notched sheet specimens as above, except internal hydrogen from molten salt electrolytes at 503 K was also examined as a variable [13]. Rapid outgassing of hydrogen, however, occurs at room temperature in ferritic stainless steels due to its high hydrogen diffusivity. Precharged specimens contained ~2 wppm residual hydrogen after testing in air, which is believed to have been trapped in the steel; most of the hydrogen (~12 wppm) outgassed from the specimens during testing [13]. Subcritical crack growth tests conducted in air on specimens with internal hydrogen showed modest effects of the trapped residual hydrogen, however, tests of precharged material in 0.11 MPa hydrogen gas resulted in similar response to tests in hydrogen without precharging. Fracture surfaces of material tested in hydrogen gas at room temperature were dominated by quasicleavage in both the hydrogen precharged and uncharged conditions [13].

3.3 Fatigue

Internal hydrogen precharging by cathodic techniques was found to increase fatigue crack growth rates and decrease the threshold stress intensity factor for crack propagation in a 12Cr-1Mo ferritic stainless steel [14]. Based on fracture mechanics testing in low-pressure hydrogen,

the degradation of fatigue properties in hydrogen gas can be expected to be greater than observed in this study.

3.4 Creep
No known published data in hydrogen gas.

3.5 Impact
No known published data in hydrogen gas.

3.6 Disk rupture testing
Fidelle et al. categorized type 430 stainless steel as having little or no sensitivity to hydrogen embrittlement during disk rupture testing [15]. This is at odds with the tensile data from the literature, perhaps due to the relative short-time scales associated with the disk rupture tests precluding substantial hydrogen transport in the lattice over the time scale of the test.

5. References

1. RA Lula. Stainless Steel (revised from "An Introduction to Stainless Steel" by JG Parr and A Hanson). Metals Park OH: American Society for Metals (1986).
2. RJ Walter and WT Chandler. Effects of High-Pressure Hydrogen on Metals at Ambient Temperature: Final Report (NASA CR-102425). Rocketdyne (report no. R-7780-1) for the National Aeronautics and Space Administration, Canoga Park CA (February 1969).
3. RP Jewitt, RJ Walter, WT Chandler and RP Frohmberg. Hydrogen Environment Embrittlement of Metals (NASA CR-2163). Rocketdyne for the National Aeronautics and Space Administration, Canoga Park CA (March 1973).
4. T-P Perng and CJ Altstetter. Effects of Deformation on Hydrogen Permeation in Austenitic Stainless Steels. Acta Metall 34 (1986) 1771-1781.
5. T-P Perng, M Johnson and CJ Altstetter. Influence of plastic deformation on hydrogen diffusion and permeation in stainless steels. Acta Metall 37 (1989) 3393-3397.
6. L-C Hwang and T-P Perng. Hydrogen transport in ferritic stainless steel under elastic stress. Mater Chem Phys 36 (1994) 231-235.
7. C-L Yu and T-P Perng. Surface effects on electrochemical hydrogen diffusion in stainless steel. Acta Metall Mater 39 (1991) 1091-1099.
8. RA Oriani. The diffusion and trapping of hydrogen in steel. Acta Metall 18 (1970) 147-157.
9. HG Nelson and JE Stein. Gas-phase hydrogen permeation through alpha iron, 4130 steel, and 304 stainless steel from less than 100°C to near 600°C (NASA TN D-7265). Ames Research Center, National Aeronautics and Space Administration, Moffett Field CA (April 1973).
10. MR Louthan and RG Derrick. Hydrogen Transport in Austenitic Stainless Steel. Corros Sci 15 (1975) 565-577.
11. XK Sun, J Xu and YY Li. Hydrogen Permeation Behaviour in Austenitic Stainless Steels. Mater Sci Eng A114 (1989) 179-187.
12. T-P Perng and CJ Altstetter. Comparison of Hydrogen Gas Embrittlement of Austenitic and Ferritic Stainless Steels. Metall Trans 18A (1987) 123-134.

13. J-H Huang and CJ Altstetter. Internal Hydrogen Embrittlement of a Ferritic Stainless Steel. Metall Mater Trans 26A (1995) 845-849.
14. GF Rodkey and RH Jones. Effect of internal hydrogen on the fatigue crack growth of a 12Cr-1Mo Steel. J Nucl Mater 155-157 (1988) 760-765.
15. J-P Fidelle, R Bernardi, R Broudeur, C Roux and M Rapin. Disk Pressure Testing of Hydrogen Environment Embrittlement. in: Hydrogen Embrittlement Testing, ASTM STP 543, American Society for Testing and Materials. (1974) p. 221-253.
16. ASTM DS-56H, Metals and Alloys in the UNIFIED NUMBERING SYSTEM (SAE HS-1086 OCT01). American Society for Testing and Materials (Society of Automotive Engineers) (2001).

Table 1.1.1. Nominal compositional ranges (wt%) of several ferritic stainless steels. [16]

UNS No.	AISI No / Common Name	Fe	Cr	Mo	Ni	Mn	Si	C	other
S40500	405	Bal	11.50 14.50	—	—	1.00 max	1.00 max	0.08 max	0.10-0.30 Al; 0.030 max S; 0.040 max P
S40900	409	Bal	10.50 11.75	—	0.50 max	1.00 max	1.00 max	0.08 max	0.75 max Ti; 0.045 max S; 0.045 max P
S42900	429	Bal	14.00 16.00	—	—	1.00 max	1.00 max	0.12 max	0.030 max S; 0.040 max P
S43000	430	Bal	16.00 18.00	—	—	1.00 max	1.00 max	0.12 max	0.030 max S; 0.040 max P
S43020	430F	Bal	16.00 18.00	0.60 max	—	1.25 max	1.00 max	0.12 max	0.15 min S; 0.060 max P
S43400	434	Bal	16.00 18.00	0.75 1.25	—	1.00 max	1.00 max	0.12 max	0.030 max S; 0.040 max P
S44800	29-4-2	Bal	28.0 30.0	3.5 4.2	2.0 2.5	0.30 max	0.20 max	0.10 max	0.020 max N; 0.020 max S; 0.025 max P

Table 1.1.2. Compositions (wt%) of several ferritic stainless steels used to study hydrogen effects.

Heat	Fe	Cr	Mo	Ni	Mn	Si	C	Other	Ref.
W69 430F†	Bal	16.33	0.40	0.24	1.07	0.63	0.096	0.07 Cu; 0.293 S; 0.015 P	[2, 3]
P87 29-4-2	Bal	29.5	3.93	2.23	0.10	0.10	0.0029	0.012 N; 0.01 P; 0.009 S	[12, 13]

† free machining grade of type 430 ferritic stainless steel with high sulfur.

Table 2.1. Permeability, diffusivity and solubility relationships for ferritic stainless steels. These relationships are plotted in Figures 2.1, 2.2 and 2.3 for permeability, diffusivity and solubility respectively.

Material	Temperature Range (K)	Pressure Range (MPa)	$\Phi = \Phi_o \exp(-E_\Phi/RT)$		$D = D_o \exp(-E_D/RT)$		$S = S_o \exp(-E_S/RT)$		Ref.
			Φ_o $\left(\dfrac{\text{mol } H_2}{\text{m} \cdot \text{s} \cdot \text{MPa}^{1/2}}\right)$	E_Φ $\left(\dfrac{\text{kJ}}{\text{mol}}\right)$	D_o $\left(\dfrac{\text{m}^2}{\text{s}}\right)$	E_D $\left(\dfrac{\text{kJ}}{\text{mol}}\right)$	S_o $\left(\dfrac{\text{mol } H_2}{\text{m}^3 \cdot \text{MPa}^{1/2}}\right)$	E_S $\left(\dfrac{\text{kJ}}{\text{mol}}\right)$	
29-4-2 (P87) Annealed	353–443	0.001–0.026	2.20 x 10⁻⁶	38.4	8.45 x 10⁻⁶	33.7	1.16	4.7	[4, 5]
	443–593				6.40 x 10⁻⁹	7.0	1534	31.4	
29-4-2 (P87) deformed 25%	383–533		2.94 x 10⁻⁶	40.3	1.71 x 10⁻⁶	36.7	1.72	3.6	[5]
29-4-2 (P87) deformed 50%	383–533		12.3 x 10⁻⁶	45.4	2.34 x 10⁻⁶	37.2	5.24	8.2	
29-4-2 (P87) deformed 75%	383–533		13.2 x 10⁻⁶	47.3	9.03 x 10⁻⁶	45.5	1.46	1.8	
Austenitic stainless steels	373-623	1x10⁻⁴ –0.03	53.5 x 10⁻⁶	56.1	0.20 x 10⁻⁶	49.3	266	6.86	[4]

Table 3.1.1.1. Smooth tensile properties of ferritic stainless steel tested at room temperature in high-pressure gaseous hydrogen.

Material	Thermal precharging	Test environment	Strain rate (s^{-1})	S_y (MPa)	S_u (MPa)	El_u (%)	El_t (%)	RA (%)	Ref.
Annealed 430F, heat W69	None	69 MPa He	0.67 x10^{-3}	496	552	—	22	64	[2, 3]
	None	69 MPa H_2		—	538	—	14	37	

Table 3.1.2.1. Notched tensile properties of ferritic stainless steel tested at room temperature in high-pressure gaseous hydrogen.

Material	Specimen	Thermal precharging	Test environment	Displace-ment rate (mm/s)	S_y (MPa)	σ_s (MPa)	RA (%)	Ref.
Annealed 430F, heat W69	(1)	None	69 MPa He	0.4 x 10^{-3}	496†	1048	1.9	[2, 3]
		None	69 MPa H_2		—	717	0.6	

† yield strength of smooth tensile bar
(1) V-notched specimen: 60˚ included angle; minimum diameter = 3.81 mm (0.15 inch); maximum diameter = 7.77 mm (0.306 inch); notch root radius = 0.024 mm (0.00095 inch). Stress concentration factor (K_t) = 8.4.
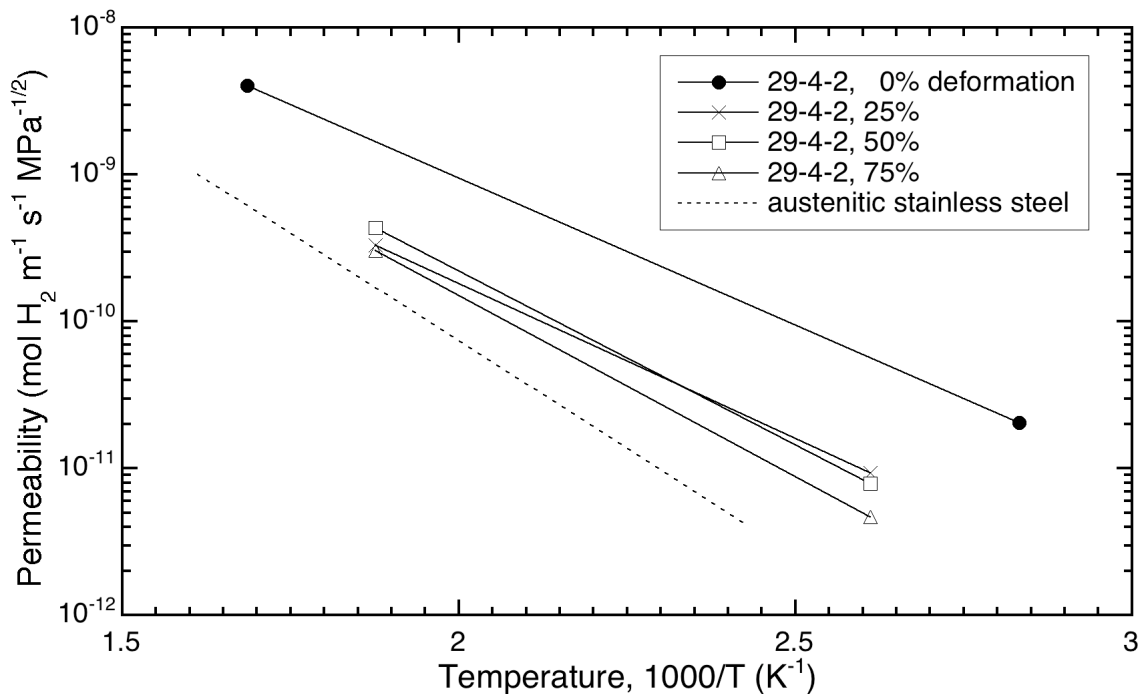

Figure 2.1. Permeability of 29-4-2 ferritic stainless steel, showing the effect of deformation on reducing permeation [5]. The dotted line represents an average permeability for several austenitic stainless alloys from Ref. [4].
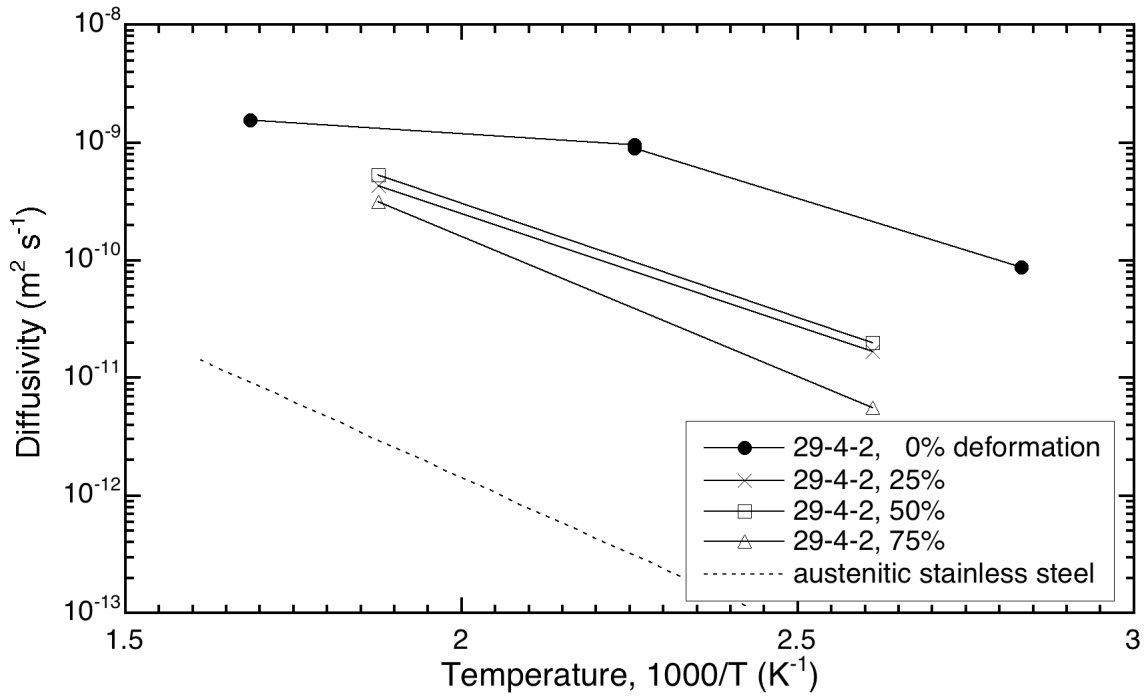
Figure 2.2. Diffusivity of 29-4-2 ferritic stainless steel, showing the effect of deformation on reducing the rate of diffusion [5]. The dotted line represents an average diffusivity for several austenitic stainless alloys from Ref. [4].
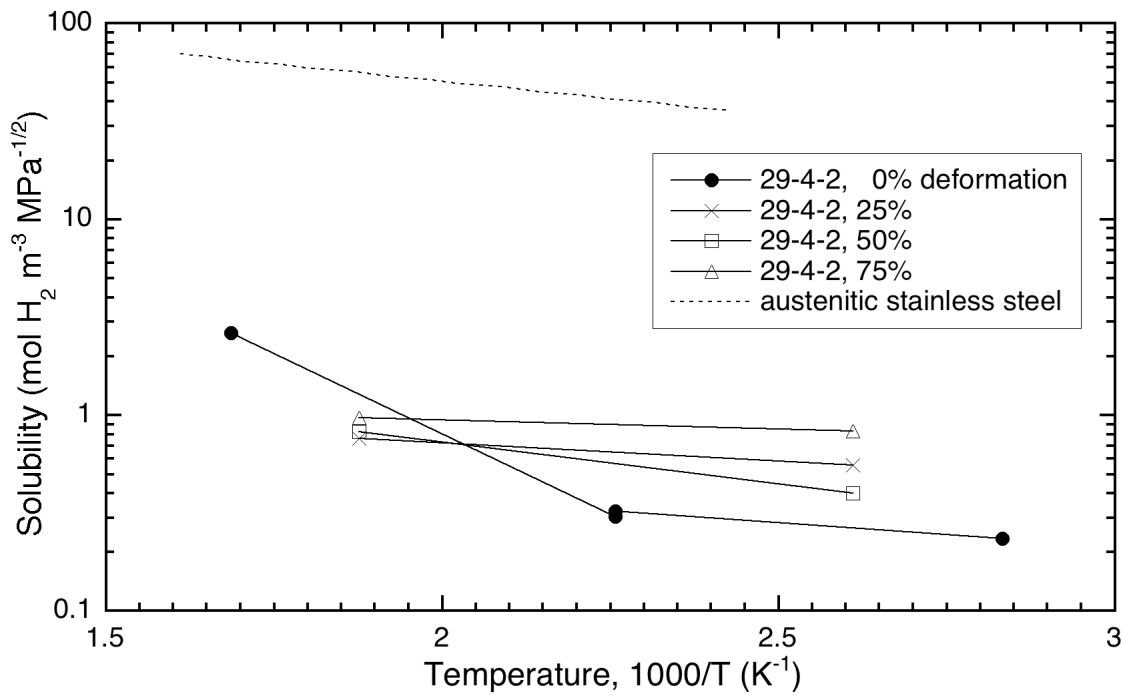

Figure 2.3. Solubility of 29-4-2 ferritic stainless steel [5]. The dotted line represents an average solubility for several austenitic stainless alloys from Ref. [4].